Investigating the Structure and Dynamics of Apo-Photosystem II

Han, Ruocheng ; Rempfer, Katharina ; Zhang, Miao ; Dobbek, Holger ; Zouni, Athina ; Dau, Holger ; Luber, Sandra

Abstract: Photosynthetic water oxidation is a model for future technologies employing solar energy to split water into hydrogen and oxygen. Natural water oxidation is carried out by a special manganese catalyst, the water-oxidizing complex (WOC), located in photosystem II (PSII) of cyanobacteria, algae, and plants. Hence, there is great interest in the molecular structure as well as structural changes during catalytic activity and assembly/disassembly of the WOC. In particular, the light-driven assembly during photosystem II repair under physiological conditions is poorly understood, and structural information about manganese depleted PSII (apo-PSII) is required as a starting point for improving this understanding. Recently Zhang et al. (eLife 2017;6:e26933) showed that the cavity harboring the WOC in PSII remains largely intact upon manganesedepletion and suggested that deprotonation of hydrogen-bonding pairs enables the charge-compensated insertion of the manganese cations without any major change of the cavity structure. By computational methods we have further investigated the structure of apo-PSII and show how it can be stabilized by protons localized at the terminal carboxylate groups inside the remaining cavity. Ab-initio molecular dynamics simulations suggest that not more than two water molecules fill the void left by manganese depletion.

DOI: https://doi.org/10.1002/cctc.201900351

Investigating the structure and dynamics of apo-Photosystem II

Ruocheng Han[1‡], Katharina Rempfer[1‡], Miao Zhang[2], Prof. Dr. Holger Dobbek[2], Prof. Dr. Athina Zouni[2], Prof. Dr. Holger Dau[3], and Prof. Dr. Sandra Luber[1*]

[1]*Institut für Chemie, Universität Zürich, Winterthurerstrasse 129, 8057 Zürich, Switzerland*
[2]*Institut für Biologie, Humboldt Universität zu Berlin, Philippstrasse 13, 10115 Berlin, Germany*
[3]*Institut für Physik, Freie Universität Berlin, Arnimallee 14, 14195 Berlin, Germany*
[*]*Corresponding author: Sandra Luber, sandra.luber@chem.uzh.ch*
[‡]*These authors contributed equally to this work.*

Abstract

Photosynthetic water oxidation is a model for future technologies employing solar energy to split water into hydrogen and oxygen. Natural water oxidation is carried out by a special manganese catalyst, the water-oxidizing complex (WOC), located in photosystem II (PSII) of cyanobacteria, algae, and plants. Hence, there is great interest in the molecular structure as well as structural changes during catalytic activity and assembly/disassembly of the WOC. In particular, the light-driven assembly during photosystem II repair under physiological conditions is poorly understood, and structural information about manganese depleted PSII (apo-PSII) is required as a starting point for improving this understanding. Recently Zhang et al. (eLife 2017;6:e26933) showed that the cavity harboring the WOC in PSII remains largely intact upon manganese-depletion and suggested that deprotonation of hydrogen-bonding pairs enables the charge-compensated insertion of the manganese cations without any major change of the cavity structure. By computational methods we have further investigated the structure of apo-PSII and show how it can be stabilized by protons localized at the terminal carboxylate groups inside the remaining cavity. *Ab-initio* molecular dynamics simulations suggest that not more than two water molecules fill the void left by manganese depletion.

Keywords— photosystem II; density functional theory; *ab-initio* molecular dynamics; protonation dynamics

1 Introduction

Efficient photochemical water oxidation can open a way to produce energy from sustainable solar power. Therefore it is of major interest to understand the mechanisms and the special structural feature of water oxidation during photosynthesis and to resolve the structure of the photosystem II (PSII)[1–4]. Of special interest is the structure and construction of

the oxygen-evolving catalyst, which plays a leading role in the process of water oxidation and is contained in the PSII. Understanding the selfassembly process of the OEC is of high importance for the development of artificial catalysts showing attractive self-assembly and self-healing properties[5–11]. Moreover, the cubane structure of the oxygen-evolving complex is an inspiration for the design of PSII mimics to gain fuels such as hydrogen from water with the aid of light. One possibility to mimic the inorganic catalyst is to use the same components it is built up from like Zhang et al. have done[12]. Another idea is to mimic the cubane structure for example with $\{Co^{II}{}_4O_4\}$[13–18] and $\{Co^{III}{}_4O_4\}$[19–21] cubanes, which have been object of experimental and computational research.

The PSII is embedded in the thylakoid membrane. Here the transformation of light into chemical energy takes place. It is a photosynthetic enzyme that uses light to split two water molecules producing molecular oxygen O_2, four protons (H^+) and four excited electrons (e^-). The PSII is a dimer and harbors in each monomer one water-oxidizing complex (WOC)[22] which has a Mn_4CaO_5-cluster core (see Fig.1 for water-oxidizing complex and the coordinating amino acids). The shape of the Mn_4CaO_5-cluster is described as a distorted chair[23]. A Mn_3CaO_4 hetero cubane cluster with an additional Mn in exo position is connected to the cubane by two μ-oxo-bridges. Further four water molecules are directly ligated to the Mn_4CaO_5-cluster, two at Mn4 and the other two at Ca^{2+} (see Fig. 1). The whole cluster is coordinated by eight amino acids from two subunits of PSII[23].

The PSII is damaged by light, therefore resynthesis is required as well as the reassembly of the Mn_4CaO_5-cluster[24]. This process can occur as frequently as every 30 minutes at full solar flux[24–26]. Reassembly of the Mn_4CaO_5-cluster of the WOC is known as photoactivation[24]. During the photoactivation of the inorganic cluster a Mn^{2+} is oxidized to Mn^{3+}/Mn^{4+}[27]. The exact way how the manganese ions return to the cavity is not clear up to now and thus also the exact procedure of reconstruction has yet to be clarified. First calculations have recently been conducted to elucidate possible initial Mn^{2+} binding sites based on energetic comparison of different structures[28]. To investigate the reassembly of the WOC, Zhang et al. removed the Mn_4CaO_5-cluster of thermophilic cyanobacteria *T. elongatus* by treating the PSII with hydroxylamin (NH_2OH), for the reduction to Mn^{2+}, and ethylenediaminetetraacetic acid (EDTA) as a chelator to fully remove the Mn^{2+}, but also Ca^{2+} ions[22], which resulted in the so-called apo-PSII. In a next step they had a closer look at the empty cavity using X-ray crystallography. Zhang et al. showed that possibly two water molecules are inside this cavity. Besides, it was shown that the net-charge and the structure of the WOC amino acids and thus the structure of the cavity are more or less conserved during the removal of the Mn_4CaO_5-cluster. The positions of all coordinated amino acid residues are largely unaffected forming a pre-organized ligand shell for kinetically competent and error-free photo-assembly of the Mn_4CaO_5-cluster[22].

In order to substitute the charges lost by removing the Mn_4CaO_5-cluster, the main idea is to place protons at the carboxylate groups of some of the terminal amino acids, whereby the positions of the protons are important for the reconstruction of the Mn_4CaO_5-cluster. Due to their positive charge and spatial extent, the protons may perturb the return of the manganese ions. However, protons can not be seen with X-Ray crystallography and that is where computational methods come into play. With the aid of density functional theory (DFT) and *ab-initio* molecular dynamics (*ab-initio* MD) we investigate various protonation patterns in order to find the best fitting arrangement of positions and number of protons conserving the structure and charge of the cavity. Elucidating this subject paves the way for in-depth understanding of the self-assembly process of the OEC, which will be instructive for design of artificial WOCs as well.

2 Methods

The Kohn–Sham DFT calculations were performed with the turbomole-7.2 software[29] using the def2-TZVP basis set and resolution of identity[30–33], the BP86 functional[34], which yields good results for structural parameters[35], and dispersion correction (DFT–D3)[36]. In addition the COSMO model[37] with a dielectric constant of $\varepsilon = 20$ was employed for the surrounding protein environment. The value of 20 for ε was chosen based on investigations of Simonson and Brooks who found that the dielectric constant is in the range of 13 to 30 in the outer part of a protein[38]. Solvent continuum models have standardly been used in previous work on PSII (see e.g. Refs.[4,39]). All energies given are electronic energies plus the COSMO correction.

Moreover, DFT-based MD (so-called *ab-initio* MD) simulations were carried out with CP2K[40]/ QUICKSTEP[41] utilizing Goedecker–Teter–Hutter (GTH)[42,43] norm-conserving pseudopotentials and DZVP-MOLOPT-SR-GTH basis sets[44]. A time step of 0.5 fs was used and the canonical sampling via velocity rescaling (CSVR) thermostat[45] in order to keep the system at the target temperature of 300 K with a 100 fs time constant run in NVT ensemble. Due to its good outcome for structural features[35,46] in all simulations the PBE exchange and correlation functional was used[47]. After equilibrating the trajectories the *ab-initio* MD was simulated for at least further 5 ps.

An input structure was extracted from the protein structure file of the apo-PSII Zhang et al. provided (PDB ID:5MX2). For reasons of resolution only the so-called locked side with lower atomic B-factors of the PSII was taken into consideration[22]. We tested model systems of varying sizes. The model finally chosen was built up from the amino acids coordinating the water oxidizing complex, namely: Asp170, Glu189, His332 Glu333, His337, Asp342, Ala344 and Glu354. In addition Leu343, to link Asp342 and Ala344, Asp61, Tyr161, Gln165, Asn181, His190, Lys317, and a chloride ion near the His332 and Arg357 residues were added. Furthermore, the two water molecules inside the cavity seen with X-ray crystallography as well as seven extra water molecules were included, see Fig. 2. The free bonds at the ends of the amino acids are saturated by hydrogen atoms. The same model systems were used for the DFT optimizations and *ab-initio* MD.

The overall net-charge of the apo-PSII has to be similar to the PSII net-charge. In order to do so, as a first guess, five protons were placed at the His332, Glu333, His337, Asp342 and Glu354 residues. Since it is highly probable that His332 and His337 residues are protonated[22], only the protonation at each of the carboxylate groups of the Glu333, Asp342 and Glu354 residue was varied, by considering two possible positions at each of the carboxylate groups, to find the most preferred proton positions within the cavity. There exist eight possible combinations to arrange the remaining three protons at the carboxylate groups of Glu333, Asp342, and Glu354.

The reference arrangement is the proton ordering Zhang et al. suggested[22], called system 0 in the following and shown in Fig. 2.

Starting from system 0, seven more systems were created (see Fig. 2), inverting the position of one or two protons at certain carboxylate groups, where inverted means that the proton is placed near the other oxygen atom of the carboxylate group:

- System 1: inverted at the carboxylate group of Glu333
- System 2: inverted at the carboxylate group of Asp342
- System 3: inverted at the carboxylate group of Glu354
- System 4: inverted at the carboxylate groups of Glu333 and Glu354
- System 5: inverted at the carboxylate groups of Asp342 and Glu333

- System 6: inverted at the carboxylate groups of Asp342 and Glu354
- System 7: inverted all protons at the carboxylate groups

The protons for the starting structure of the calculations are placed in such a way that they face inside the cavity or a near oxygen atom and the distance to the carboxylate oxygen is 0.96 Å.

3 Results and Discussion

We started the investigation with structure optimizations with DFT and *ab-initio* MD of the systems 0 to 7. In both cases the atoms of the backbone were fixed, only the residues of the coordinating amino acids, additional water molecules, and all hydrogen atoms were able to move. Next, the distances and mean values, respectively, between certain oxygen atoms of the amino acid carboxylate groups were determined and compared to the distances measured in the X-ray crystallography by Zhang et al. (see Fig. 3). Due to the error of measurement (2.0 Å resolution), all distances with a difference less or equal 0.4 Å to the distances given by Zhang et al. have been taken to be in agreement with the experimental data.

The resulting distances after the optimization with five protons are presented in table 1.

Each of the systems exhibits at least one distance that deviates noteworthy from the crystal structure after optimization with DFT. System 7 shows a considerable deviation for one distance and has the highest energy of all systems with an energy of ca. +18 kcal/mol above the energy of system 0, which is the system with the lowest energy. System 3 has also only one distance that deviates by the same amount. Its energy is 2 kcal/mol lower compared to the energy of system 0. Evaluation of the proton motion inside the cavity, observed in the *ab-initio* MD trajectories, depicts that a proton transfer from the nearby water or the carboxylate group of Glu354 residue to the carboxylate group of the terminal Ala344 residue occurs.

During the catalytic cycle in photosynthesis, the charge of the manganese ions of the inorganic cluster changes. In the S_1-state (dark adapted state of the Mn cluster) one Ca^{2+}, two Mn^{3+}, two Mn^{4+}, and five O^{2-} ions are existent. Adding up the charges of the ions in the WOC core results in a positive net-charge of +6. Since the net-charge should be nearly conserved in the apo-PSII insertion of about five to seven protons in the cavity is advisable. Taking this and the behavior seen in *ab-initio* MD into account, it appears reasonable to suppose that there is an additional proton at the carboxylate group of Ala344, so that now six protons are inside the cavity introducing six positive charges. Although a tendency of the proton transfer to only one oxygen atom (called OXT in the following, see Fig. 3) of the two of the Ala344 residue was observed we investigated both possible proton positions at the Ala344, in DFT optimization and *ab-initio* MD. So in each of the systems an additional proton was placed at the Ala344 residue (see Fig. 3).

Nevertheless, after adding an additional proton at the O or OXT atom of the Ala344 residue (see Fig. 3 for nomenclature), each expanded system has at least one clearly deviating distance after optimization with DFT (tables 2 and 3).

Once again the proton behavior during the *ab-initio* MD runs is remarkable. A proton was transferred to Glu189 from Asp342 or His337, respectively, if the proton of Asp342 was not facing the Glu189 residue. Having regard to this and the fact that Bucher et al. showed that in the KcsA potassium channel the Glu71 and Asp80 residues share a proton which has a tendency to stay at Glu71[48], two new possible arrangement types came up,

one placing the proton at the Glu189 residue instead of Asp342 (6 protons) and another one with an additional proton at Glu189 (7 protons). In both cases the protonation at the Ala344 residue remained conserved. However, bringing the proton to the Glu189 residue instead of Asp342 did not improve the results in any of the expanded systems.

Finally, the case of seven protons was examined. As an example for such a proton arrangement expanded system 6 before the geometry optimization is shown in Fig. 4 on the left. After optimization, this modified system 6 shows a low energy and there is no distance deviating more than the error of measurement after the optimization (see table 4 and Fig. 4 (right) for an overlay with the X-ray structure). The energy after optimization is only 0.1 kcal/mol higher than the one of system 3, the one with the lowest energy. System 7 exhibits no distance deviating more than the error of experimental measurement, too. Nevertheless the energy of system 7 is significantly higher than the energy of system 3 leading to the fact that system 7 has again the highest energy.

It is noteworthy that expanded systems 6 and 7 have the same ratio syn to anti protonation, where the number of energetically less favorable anti-protonation[49] is larger compared to the favorable syn-protonation.

Table 5 shows the information of proton transfer observed during geometry optimizations. It is not surprising that such phenomena appear, and proton redistributions largely reflect what was mentioned earlier. One may notice that for some expanded systems, proton transfer happens from Glu333 to Asp61, which has been regarded as part of a proton channel (see, e.g., Refs.[50,51]). Expanded system 6 shown in table 4 which has been found to be the system with low energy and distances not strongly deviating from the X-ray structure has thus only six protons in the cavity after the optimization. From this system, we also removed the proton at the Asp61 residue and optimized the structure. All distances were found not to deviate noteworthy from the X-ray structure. Test calculations were also carried out for the expanded (6-proton) systems given in Table 3 and an additional proton at the Asp61 residue where again such expanded systems 6 and 7 showed the smallest deviation from the X-ray structure.

In this context an interesting observation was made when the distance between the proton at His332 and an oxygen atom of one water molecule inside the cavity was constrained during the *ab-initio* MD with system 0 and an additional proton at the OXT atom of Ala344 residue (six protons in the cavity; see Fig. 5 (left) for overlay with X-ray data). Here again the proton was transferred to Glu189 and the missing proton at Asp342 was then transferred from His337 to Asp342 (see Fig. 5 on the right). During the MD, the carboxylate group of Glu354 performed nearly a 180° turn. Table 6 shows distance information from the *ab-initio* MD simulation.

When now the inverse oxygen atom is used for the distance determination from Glu354 residue to the Asp342 or Glu333 residue, the average values do not deviate much from the values measured inside the crystal. As an example the distance between the oxygen atoms Zhang et al. specified and between the other oxygen of the carboxylate group of Glu354 and Glu333 is presented in Fig. 6. Histograms showing the distance distribution are illustrated in Fig. 7. Also, the obtained proton pattern contains protonated Glu189, which matches what we have proposed in table 4. This is a further indication that a system with six protons inside the cavity might be a preferred arrangement.

In the crystal structure two oxygen atoms belonging to water are observed inside the cavity. To ensure this is not a coincidence a third water molecule was placed inside the cavity. This water molecule was not fixed and could move freely during the simulations. The final distances after optimization can be seen in table 7.

Astonishingly, in some cases single distances are even better than without the third water molecule. Also striking is that the distances between His332 and Asp342 always differ significantly from the distances measured in the crystal structure. When monitoring the movement of the additional third water molecule it seems as if the water molecule pulls the carboxylate group of Glu189 and the hydrogen atoms of the two other water molecules outwards leading to a rotation of the water molecules and a rearrangement of the amino acid residues. This can be observed for example in the case of system 6 (see Fig. 8). For other proton arrangements within the cavity, for example system 4, a proton exchange takes place between the additional water molecule and the other water molecules outside the cavity, which in turn release a proton to another near water or a carboxylate group. Also during an *ab-initio* MD run with three instead of two water molecules in the cavity proton transfers between single water molecules and carboxylate groups can be observed. However, the additional water molecule does not remain in the cavity but leaves it and the carboxylate group of the Glu189 residue is slightly rotated. Through proton transfer and rotation of carboxylate groups, the amino acids finally orient in such a way that the distances between them are as close as possible to those in the crystal, but not necessarily with the proton arrangement that was given at the beginning (see Fig. 8).

4 Conclusion

We computationally investigated the structure of the apo-photosystem II aiming at a better understanding of the reassembly of the water-oxidizing complex, which is of high interest for design of artificial WOCs featuring attractive reassembly and self-healing properties. For this purpose we modified the X-ray structure of the apo-PSII of thermophilic cyanobacteria *T. elongatus* recently published by Zhang et al. in 2017[22] (PDB ID: 5MX2) by introducing protons into the empty cavity to find proton arrangements which stabilize the structure of the "empty" cavity. Assuming that both histidine residues His332 and His337 are protonated due to neighboring carboxylate groups, only the terminal carboxylate groups of Glu189, Glu333, Asp342, Ala344, and Glu354 were protonated as initial guess for the calculations.

We started our investigation with five protons at eight different positions of the carboxylate groups of Glu333, Asp342, and Glu354. In accordance with likely charges inside the cavity, we increased the number of protons from five to six and seven respectively, based on the observation of proton transfers to the Glu189 and Ala344 residue in the *ab-initio* MD trajectories. So we were able to identify possible proton placements conserving the structure, namely expanded (7-proton) system 7 and expanded system 6 with seven protons (six protons after the optimization) inside the cavity, i.e. additional protons at Ala344 (OXT atom) and Glu189 compared to the start system. The latter system would support the theory that during the reassembly of the Mn_4CaO_5-cluster the Mn^{2+} ion first moves to the Mn4 position[22] since the protons are far enough away from the possible pathway of the ion to the Mn4 position. Nevertheless, the *ab-initio* MD trajectories at 300 K made clear that apo-PSII has a flexible structure with several possible proton patterns energetically and structurally similar to each other, since proton transfers and flipping of the carboxylate groups to other arrangements can be observed.

Furthermore, our calculations indicate that an additional water molecule inside the cavity may be unlikely, since the cavity is strongly deformed in our test calculations when bringing a third water molecule inside it. In addition, the third water molecule leaves the cavity during the *ab-initio* MD simulation. This result suggests that two water molecules

presumably participate in the formation of the μ-oxo bridges and interconnect the two Mn ions occupied at the Mn1 and Mn2 sites. Accordingly, the μ-oxo bridges and the two ions can form a binuclear (Mn1-(μ-O)2-Mn2) intermediate during the cluster-assembly (Zhang et al, 2017). In order to gain more detailed insight, further calculations are required in the future.

5 Acknowledgment

This work has been supported by the University Research Priority Program "Solar Light to Chemical Energy Conversion" (LightChEC), the Clara-Immerwahr-Award of Unicat Excellence cluster and the Swiss National Science Foundation (grant. No. PP00P2_170667). The computations reported in this paper have been supported by the Swiss National Supercomputing Center, accounts s745 and s788. Further we thank the Deutsche Forschungsgemeinschaft (DFG) for financial support to the collaborative research center on Protonation Dynamics in Protein Function (SFB 1078, projects A4-Dau and A5-Zouni/Dobbek) and UniSysCat funded by the Deutsche Forschungsgemeinschaft (DFG, German Research Foundation) under Germany's Excellence Strategy - EXC/1 (UniSysCat) - 390540038.

References

[1] M. Askerka, G. W. Brudvig, V. S. Batista, *Acc. Chem. Res.* **2017**, *50*, 41–48.

[2] J. P. McEvoy, G. W. Brudvig, *Chem. Rev.* **2006**, *106*, 4455–4483.

[3] J. Barber, *Chem. Soc. Rev.* **2009**, *38*, 185–196.

[4] W. Ames, D. A. Pantazis, V. Krewald, N. Cox, J. Messinger, W. Lubitz, F. Neese, *J. Am. Chem. Soc.* **2011**, *133*, 19743–19757.

[5] H. Dau, C. Limberg, T. Reier, M. Risch, S. Roggan, P. Strasser, *ChemCatChem* **2010**, *2*, 724–761.

[6] I. Zaharieva, P. Chernev, M. Risch, K. Klingan, M. Kohlhoff, A. Fischer, H. Dau, *Energy Environ. Sci.* **2012**, *5*, 7081–7089.

[7] I. Zaharieva, D. González-Flores, B. Asfari, C. Pasquini, M. R. Mohammadi, K. Klingan, I. Zizak, S. Loos, P. Chernev, H. Dau, *Energy Environ. Sci.* **2016**, *9*, 2433–2443.

[8] D. A. Lutterman, Y. Surendranath, D. G. Nocera, *J. Am. Chem. Soc.* **2009**, *131*, 3838–3839.

[9] M. W. Kanan, D. G. Nocera, *Science* **2008**, *321*, 1072–1075.

[10] M. W. Kanan, Y. Surendranath, D. G. Nocera, *Chem. Soc. Rev.* **2009**, *38*, 109–114.

[11] D. G. Nocera, *Acc. Chem. Res.* **2012**, *45*, 767–776.

[12] C. Zhang, C. Chen, H. Dong, J. Shen, H. Dau, J. Zhao, *Science* **2015**, *348*, 690–693.

[13] Evangelisti, F. and Güttinger, R. and Moré, R. and Luber, S. and Patzke, G. R., *J. Am. Chem. Soc.* **2013**, *135*, 18734–18737.

[14] F. Evangelisti, R. Moré, F. Hodel, S. Luber, G. R. Patzke, *J. Am. Chem. Soc.* **2015**, *137*, 11076–11084.

[15] F. H. Hodel, S. Luber, *ACS Catal.* **2016**, *6*, 1505–1517.

[16] F. H. Hodel, S. Luber, *ACS Catal.* **2016**, *6*, 6750–6761.

[17] M. Schilling, F. Hodel, S. Luber, *ChemSusChem* **2017**, *10*, 4561–4569.

[18] F. Song, R. Moré, M. Schilling, G. Smolentsev, N. Azzaroli, T. Fox, S. Luber, G. R. Patzke, *J. Am. Chem. Soc.* **2017**, *139*, 14198–14208.

[19] N. S. McCool, D. M. Robinson, J. E. Sheats, G. C. Dismukes, *J. Am. Chem. Soc.* **2011**, *133*, 11446–11449.

[20] J. G. McAlpin, T. A. Stich, C. A. Ohlin, Y. Surendranath, D. G. Nocera, W. H. Casey, R. D. Britt, *J. Am. Chem. Soc.* **2011**, *133*, 15444–15452.

[21] S. Berardi, G. La Ganga, M. Natali, I. Bazzan, F. Puntoriero, A. Sartorel, F. Scandola, S. Campagna, M. Bonchio, *J. Am. Chem. Soc.* **2012**, *134*, 11104–11107.

[22] M. Zhang, M. Bommer, R. Chatterjee, R. Hussein, J. Yano, H. Dau, J. Kern, H. Dobbek, A. Zouni, *eLife* **2017**, *6*, year.

[23] Y. Umena, K. Kawakami, J. Shen, N. Kamiya, *Nature* **2011**, *473*, 55–60.

[24] J. Dasgupta, G. M. Ananyev, G. C. Dismukes, *Coord. Chem. Rev.* **2008**, *252*, 347–360.

[25] E. Zak, B. Norling, R. Maitra, F. Huang, B. Andersson, H. B. Pakrasi, *Proceedings of the National Academy of Sciences* **2001**, *98*, 13443–13448.

[26] N. Keren, A. Berg, P. J. M. van Kan, H. Levanon, I. Ohad, *Proc. Natl. Acad. Sci. U. S. A.* **1997**, *94*, 1579–1584.

[27] M. M. Najafpour, G. Renger, M. Hołyńska, A. N. Moghaddam, E. Aro, R. Carpentier, H. Nishihara, J. J. Eaton-Rye, J. Shen, S. I. Allakhverdiev, *Chem. Rev.* **2016**, *116*, 2886–2936.

[28] R. J. Debus, *Chem. Phys. Lett.* **2019**, *721*, 62–67.

[29] *TURBOMOLE V7.0 2015, a development of University of Karlsruhe and Forschungszentrum Karlsruhe GmbH, 1989-2007, TURBOMOLE GmbH, since 2007; available from* `http://www.turbomole.com`.

[30] F. Weigend, *Phys. Chem. Chem. Phys.* **2002**, *4*, 4285–4291.

[31] M. Sierka, A. Hogekamp, R. Ahlrichs, *J. Chem. Phys.* **2003**, *118*, 9136–9148.

[32] K. Eichkorn, F. Weigend, O. Treutler, R. Ahlrichs, *Theor. Chem. Acc.* **1997**, *97*, 119–124.

[33] K. Eichkorn, O. Treutler, H. Öhm, M. Häser, R. Ahlrichs, *Chem. Phys. Lett.* **1995**, *242*, 652 – 660.

[34] A. D. Becke, *Phys. Rev. A* **1988**, *38*, 3098–3100.

[35] M. Orio, D. A. Pantazis, F. Neese, *Photosynthesis Research* **2009**, *102*, 443–453.

[36] S. Grimme, J. Antony, S. Ehrlich, H. Krieg, *J. Chem. Phys.* **2010**, *132*, 154104.

[37] A. Klamt, G. Schüürmann, *J. Chem. Soc. Perkin Trans. 2* **1993**, 799–805.

[38] T. Simonson, C. L. Brooks, *J. Am. Chem. Soc.* **1996**, *118*, 8452–8458.

[39] P. E. Siegbahn, *Biochim. Biophys. Acta Bioenerg.* **2013**, *1827*, 1003 – 1019.

[40] `http://cp2k.org/`, [CP2K Version 5.0 (Development Version)].

[41] J. VandeVondele, M. Krack, F. Mohamed, M. Parrinello, T. Chassaing, J. Hutter, *Comput. Phys. Commun.* **2005**, *167*, 103–128.

[42] S. Goedecker, M. Teter, J. Hutter, *Phys. Rev. B* **1996**, *54*, 1703–1710.

[43] C. Hartwigsen, S. Goedecker, J. Hutter, *Phys. Rev. B* **1998**, *58*, 3641–3662.

[44] J. VandeVondele, J. Hutter, *J. Chem. Phys.* **2007**, *127*, 114105.

[45] G. Bussi, D. Donadio, M. Parrinello, *J. Chem. Phys.* **2007**, *126*, 014101.

[46] Y. Takano, A. Kusaka, H. Nakamura, *Biophys. Physicobiol.* **2016**, *13*, 27–35.

[47] J. P. Perdew, K. Burke, M. Ernzerhof, *Phys. Rev. Lett.* **1996**, *77*, 3865–3868.

[48] D. Bucher, L. Guidoni, U. Rothlisberger, *Biophys. J.* **2007**, *93*, 2315–2324.

[49] L. D'Ascenzo, P. Auffinger, *Acta Crystallogr. Sect. B: Struct. Sci. Cryst. Eng. Mater.* **2015**, *71*, 164–175.

[50] R. J. Debus, *Biochemistry* **2006**, *45*, 2063–2071.

[51] R. J. Debus, *Biochemistry* **2014**, *53*, 2941–2955.

Table 1: Distances (in Å) and relative energies after optimization with DFT for the model system with five protons in the cavity: Displayed in red are the distances that deviate more than 0.4 Å from the distances measured with X-ray crystallography. The relative energies $E_{relative}$ are calculated as $E_{relative} = E_i - E_0, i = 1,\ldots,7$, where E_i is the energy of system $i = 1,\ldots,7$ and E_0 the energy of system 0. Further the ratio syn to anti protonated carboxylate groups after optimization is shown.

Distance	sys. 0	sys. 1	sys. 2	sys. 3	sys. 4	sys. 5	sys. 6	sys. 7	crystal
Asp342−His332	4.3	4.4	3.7	3.8	3.8	3.7	3.4	3.8	3.3
Asp342−His337	2.6	2.5	2.8	2.6	2.6	3.8	3.6	3.1	2.7
Asp342−Glu189	2.6	2.5	3.4	2.6	2.5	3.5	3.4	3.3	2.9
Asp342−Glu354	3.5	3.5	3.2	3.1	3.0	3.1	2.9	2.9	3.0
Glu354−Glu333	2.9	3.1	3.0	2.6	3.3	3.2	2.5	3.2	2.8
Glu189−His332	3.4	3.5	2.5	3.3	3.8	2.6	2.6	2.6	3.0
Asp170−Glu333	4.8	4.9	5.1	4.7	5.0	4.8	5.5	4.8	4.4
$E_{relative}$ [kcal/mol]	0.0	8.1	8.0	-2.2	9.2	15.7	9.9	18.0	
syn/anti protonation	2/1	2/1	2/1	2/1	2/1	2/1	1/2	2/1	

Table 2: Distances (in Å) and relative energies after optimization with DFT for all systems with an additional proton at O atom of the Ala344 residue (see Fig. 3). Overall six protons were added in the cavity. Displayed in red are the distances that deviate more than 0.4 Å from the distances measured with X-ray crystallography. The relative energies $E_{relative}$ are calculated as $E_{relative} = E_i - E_0, i = 1,\ldots,7$, where E_i is the energy of system $i = 1,\ldots,7$ and E_0 the energy of system 0. Further the ratio syn to anti protonated carboxylate groups after optimization is shown.

Distance	sys. 0	sys. 1	sys. 2	sys. 3	sys. 4	sys. 5	sys. 6	sys. 7	crystal
Asp342−His332	4.1	3.9	3.8	3.8	3.9	3.8	4.2	3.5	3.3
Asp342−His337	2.5	2.5	2.9	2.5	2.5	2.9	3.8	2.9	2.7
Asp342−Glu189	2.5	2.5	3.3	2.5	2.5	3.6	5.3	3.8	2.9
Asp342−Glu354	4.0	3.7	3.1	3.7	3.7	3.0	3.1	3.2	3.0
Glu354−Glu333	4.1	3.5	4.5	3.8	2.8	3.4	2.7	2.8	2.8
Glu189−His332	2.9	2.9	2.6	2.8	2.9	2.6	2.6	2.6	3.0
Asp170−Glu333	4.6	4.6	4.6	4.5	4.7	4.8	4.6	4.6	4.4
$E_{relative}$ [kcal/mol]	0.0	-16.6	1.6	-13.7	-14.3	8.0	-16.5	-2.9	
syn/anti protonation	3/1	3/1	3/1	3/1	3/1	3/1	2/2	2/2	

Table 3: Distances (in Å) and relative energies after optimization with DFT for all systems with an additional proton at OXT atom of the Ala344 residue (see Fig. 3). Overall six protons were added in the cavity. Displayed in red are the distances that deviate more than 0.4 Å from the distances measured with X-ray crystallography. The relative energies $E_{relative}$ are calculated as $E_{relative} = E_i - E_0, i = 1,\ldots,7$, where E_i is the energy of system $i = 1,\ldots,7$ and E_0 the energy of system 0. Further the ratio syn to anti protonated carboxylate groups after optimization is shown.

Distance	sys. 0	sys. 1	sys. 2	sys. 3	sys. 4	sys. 5	sys. 6	sys. 7	crystal
Asp342−His332	3.9	3.9	3.6	3.8	3.9	3.5	3.4	3.4	3.3
Asp342−His337	2.6	2.5	4.2	2.6	2.5	4.3	3.3	3.2	2.7
Asp342−Glu189	2.5	2.5	3.6	2.5	2.5	3.5	3.4	3.4	2.9
Asp342−Glu354	3.8	3.7	3.7	3.5	3.6	3.8	3.0	3.1	3.0
Glu354−Glu333	4.5	4.0	5.2	2.6	2.7	3.9	2.6	2.7	2.8
Glu189−His332	2.7	2.8	3.6	2.7	2.8	2.7	2.7	2.7	3.0
Asp170−Glu333	4.7	4.6	4.6	4.7	4.6	4.7	4.6	4.7	4.4
$E_{relative}$ [kcal/mol]	0.0	-8.3	-10.8	-25.6	-11.6	-7.8	-18.3	-11.4	
syn/anti protonation	3/1	3/1	3/1	3/1	3/1	3/1	3/1	3/1	

Table 4: Distances (in Å) and relative energies after optimization with DFT with an additional proton at OXT of Ala344 except for system 5 where it is at the O atom of the Ala344 carboxylate group. Further an additional proton at one oxygen atom of Glu189 was introduced. Overall seven protons were added in the cavity. Displayed in red are the distances that deviate more than 0.4 Å from the distances measured with X-ray crystallography. The relative energies $E_{relative}$ are calculated as $E_{relative} = E_i - E_0, i = 1,\ldots,7$, where E_i is the energy of system $i = 1,\ldots,7$ and E_0 the energy of system 0. Further the ratio syn to anti protonated carboxylate groups after optimization is shown.

Distance	sys. 0	sys. 1	sys. 2	sys. 3	sys. 4	sys. 5	sys. 6	sys. 7	crystal
Asp342−His332	4.8	4.7	3.8	4.1	4.7	3.9	3.7	3.7	3.3
Asp342−His337	2.8	2.7	3.1	2.6	2.7	3.0	3.1	3.0	2.7
Asp342−Glu189	3.8	2.9	2.7	2.7	2.7	2.7	2.7	2.7	2.9
Asp342−Glu354	4.0	4.2	4.1	4.3	4.0	3.1	3.0	3.0	3.0
Glu354−Glu333	3.7	3.3	4.4	2.6	3.0	3.4	2.5	2.6	2.8
Glu189−His332	3.7	3.7	3.1	2.9	3.2	3.0	3.2	3.0	3.0
Asp170−Glu333	4.9	4.5	4.7	4.9	4.4	4.6	4.7	4.7	4.4
$E_{relative}$ [kcal/mol]	0.0	-16.7	-5.0	-25.1	-12.1	-3.2	-25.0	3.0	
syn/anti protonation	2/3	4/1	1/4	4/1	4/1	3/2	2/3	2/3	

Table 5: Proton transfer during geometry optimization of the 5-proton (table 1), 6-proton (O) (table 2), 6-proton (OXT) (table 3), and 7-proton (table 4) systems. "w" represents one water molecule and "w2" refers to two water molecules with a transfer from one to the other water molecule (i.e. w → w).

System	5-proton	6-proton (O)	6-proton (OXT)	7-proton
sys. 0	His332 → w2 → Ala344 Asp342 → Glu189	Asp342 → Glu189	None	None
sys. 1	His332 → w2 → Ala344 Asp342 → Glu189	Asp342 → Glu189	Asp342 → Glu189	None
sys. 2	His332 → Glu189	His332 → Glu189	Ala344 → w → Glu189	Glu333 → w2 → Asp61
sys. 3	Glu354 → w → Ala344 Asp342 → Glu189	Asp342 → Glu189 Ala344 → w2	Glu333 → w2 → Asp61	Glu333 → w2 → Asp61
sys. 4	Asp342 → Glu189	Asp342 → Glu189	Asp342 → Glu189	None
sys. 5	None	His332 → Glu189 Asp344 → w → Asp170	Ala344 → w → Glu189	None
sys. 6	Glu354 → w → Ala344 His332 → Glu189	His332 → Glu189 Glu333 → w2 → Asp61	Ala344 → w → Glu189	Glu333 → w2 → Asp61
sys. 7	His332 → Glu189	His332 → Glu189 Asp344 → w	Ala344 → w → Glu189	None

Table 6: Distances (in Å) and their standard deviations during *ab-initio* MD. Displayed in red are the distances that deviate more than 0.4 Å from the distances measured with X-ray crystallography.

Distance	*ab-initio* MD	crystal
Asp342−His332	3.2 ± 0.2	3.3
Asp342−His337	3.7 ± 0.3	2.7
Asp342−Glu189	2.8 ± 0.2	2.9
Asp342−Glu354	3.0 ± 0.2	3.0
Glu354−Glu333	2.9 ± 0.2	2.8
Glu189−His332	3.2 ± 0.2	3.0
Asp170−Glu333	4.8 ± 0.2	4.4

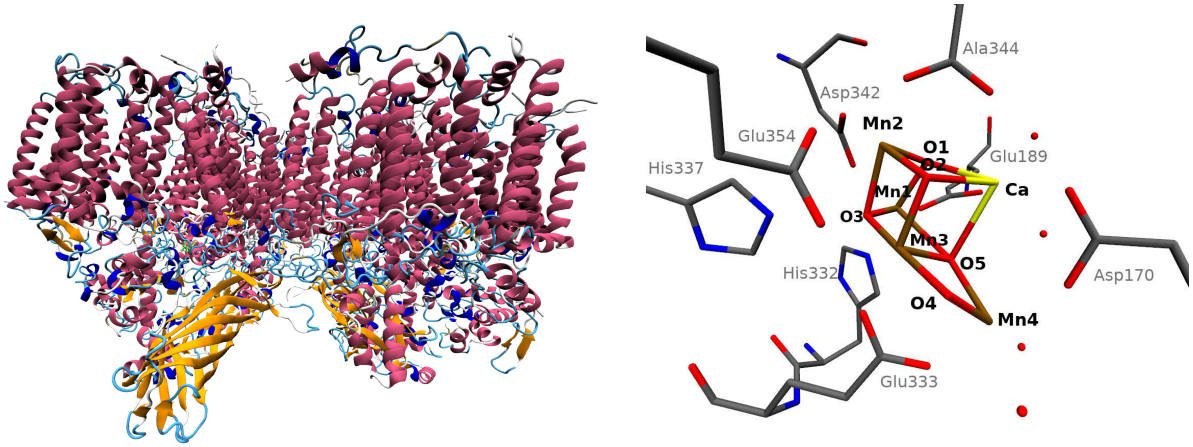

Figure 1: The photosystem II structure of thermophilic cyanobacteria *Thermosynechococcus vulcanus* (left) and a moiety of the so-called water-oxidizing complex (WOC): eight amino acids of the cavity coordinating the Mn_4CaO_5-cluster built up from one calcium, four manganese and five oxygen atoms and four water oxygen atoms (oxygen atoms displayed in red)[23]. For reasons of clarity no hydrogen atoms are added (PDB ID:3WU2).

Table 7: Distances (in Å) and relative energies after optimization with DFT with an additional water molecule inside the cavity and five protons in the cavity. Displayed in red are the distances that deviate more than 0.4 Å from the distances measured with X-ray crystallography. The relative energies $E_{relative}$ are calculated as $E_{relative} = E_i - E_0, i = 1,\ldots,7$, where E_i is the energy of system $i = 1,\ldots,7$ and E_0 the energy of system 0. Further the ratio syn to anti protonated carboxylate groups after optimization is shown.

Distance	sys. 0	sys. 1	sys. 2	sys. 3	sys. 4	sys. 5	sys. 6	sys. 7	crystal
Asp342−His332	3.9	3.9	4.4	3.9	3.8	4.1	4.3	4.2	3.3
Asp342−His337	2.5	2.6	2.8	2.6	2.6	2.9	3.1	2.9	2.7
Asp342−Glu189	2.5	2.5	4.9	2.5	2.5	4.3	5.6	4.2	2.9
Asp342−Glu354	3.3	3.3	3.0	3.2	3.5	3.0	3.1	3.1	3.0
Glu354−Glu333	2.7	3.0	3.1	2.5	3.6	3.2	3.2	3.5	2.8
Glu189−His332	3.4	3.6	2.6	3.6	3.3	2.6	2.6	2.6	3.0
Asp170−Glu333	4.9	4.6	4.8	4.7	5.3	4.7	4.9	4.7	4.4
$E_{relative}$ [kcal/mol]	0.0	-2.8	17.2	-1.4	1.2	16.0	-0.5	-1.6	
syn/anti protonation	2/1	2/1	2/1	2/1	2/1	2/1	1/2	2/1	

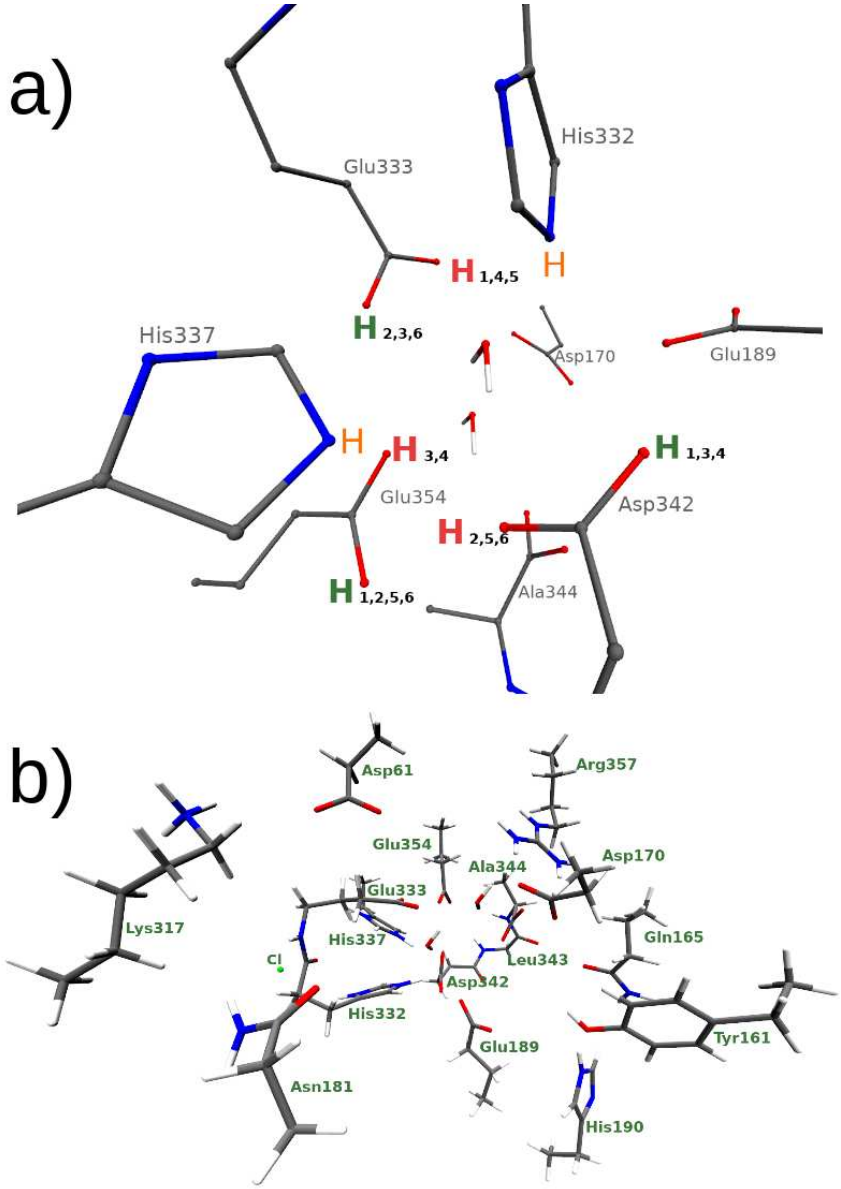

Figure 2: a) The depleted cavity formed by the coordinating amino acids. Shown are the protons that are not moved during the investigations (in orange), the protons at the amino acid residues as Zhang et al. (system 0)[22] suggested (in green) and the protons inverse to the suggestion of Zhang et al. (system 7 in red). The small black numbers indicate the proton positions of the remaining systems 1 to 6. Furthermore the two water molecules observed inside the cavity are shown (PDB ID:5MX2). b): All amino acids taken into account in the calculations.

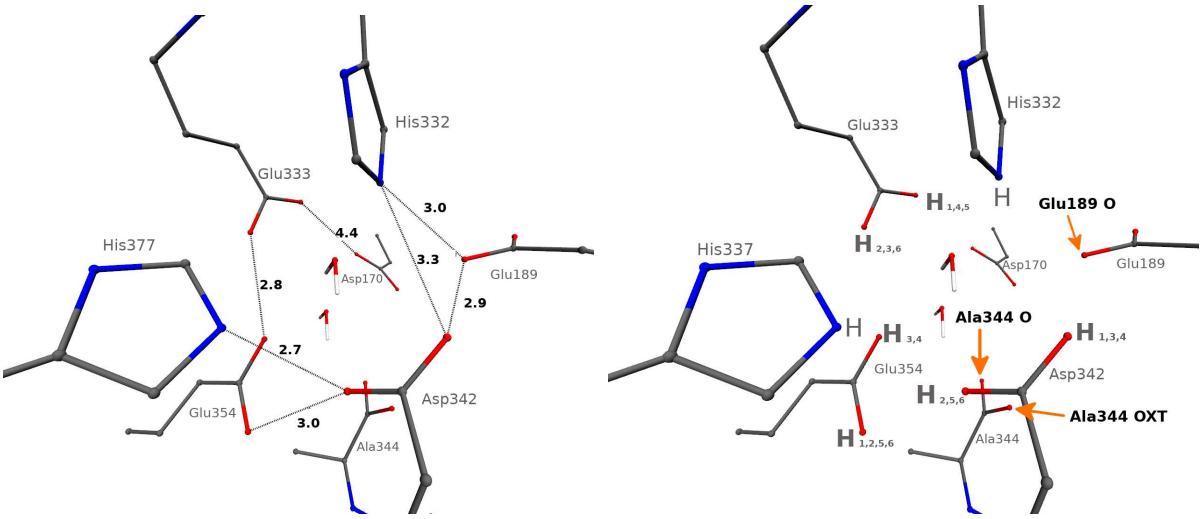

Figure 3: Distances (in Å) that Zhang et al.[22] measured in the crystal structure (left) and the atoms where additional protons were placed indicated by arrows (right) (PDB ID:5MX2).

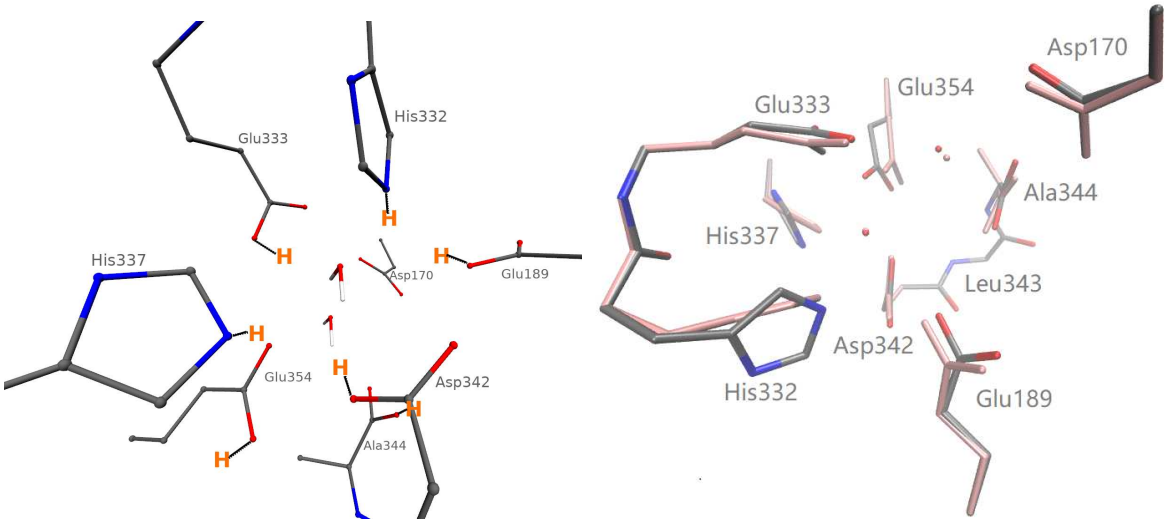

Figure 4: Expanded system 6 with seven protons before optimization (left). The overlay of the system after optimization (in color) and the structure from X-ray crystallography (in pink) (right). In addition to the carboxylate groups Zhang et al. suggested, the carboxylate groups of the terminal Ala344 and Glu189 residues were protonated.

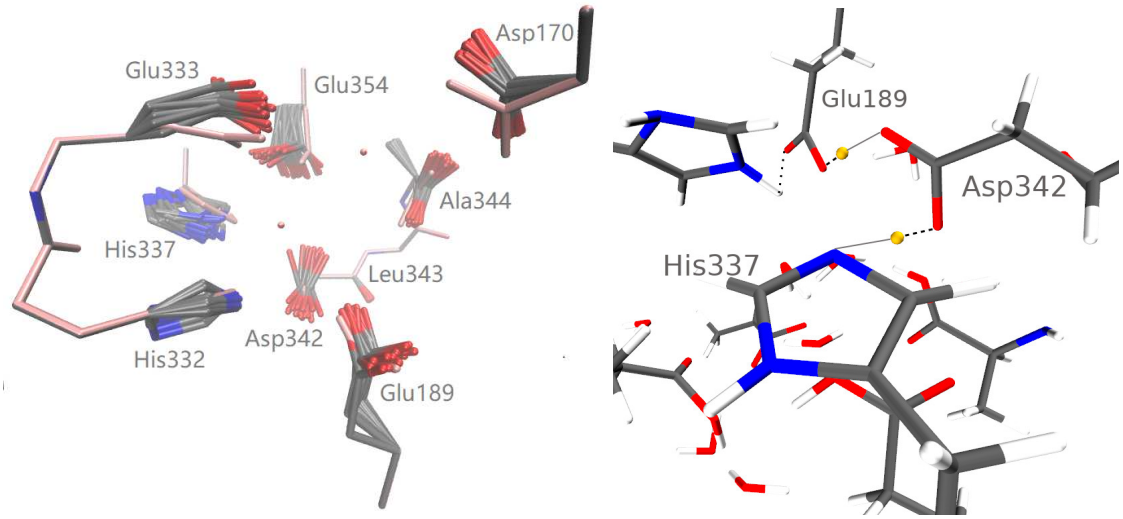

Figure 5: Overlay of snapshots from the *ab-initio* MD trajectory (in color) and the structure from X-ray crystallography (in pink) (left). The proton transfer process during the simulation (right). The yellow marked hydrogen atoms are transferred during the MD run, when the distance between the proton at His332 and an oxygen atom of one water molecule inside the cavity was constrained.

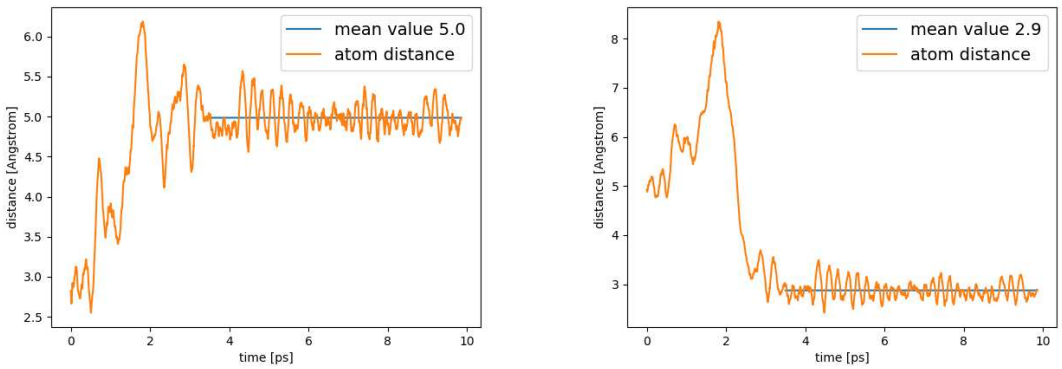

Figure 6: Distance of Glu333 and Glu354 in the course of a trajectory measured between the oxygen atoms Zhang et al. specified (left) and between the other oxygen of the carboxylate group of Glu354 and Glu333 (right). The mean value of the distances is calculated taking into account all distances after the rotation of the carboxylate group is finished. The blue line representing the mean value indicates what part of the trajectory was used for determination of the mean value.

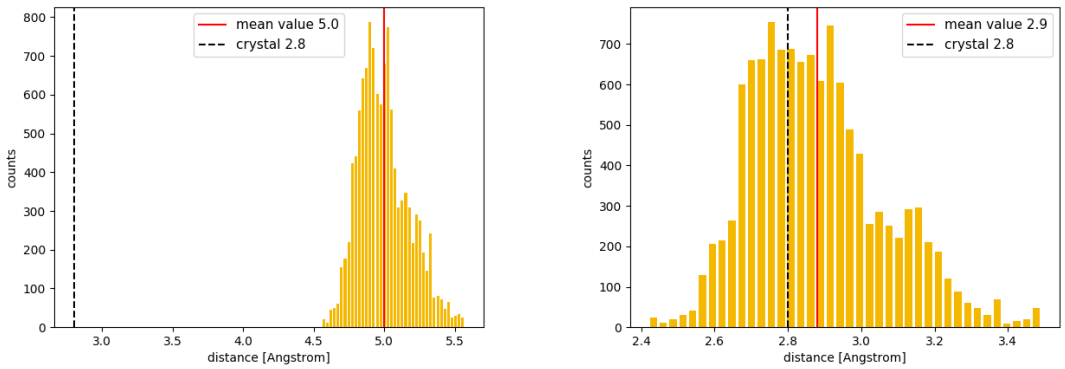

Figure 7: Distribution and mean value of distance between Glu333 and Glu354 measured between the oxygen atoms Zhang et al. specified (left) and between the other oxygen of the carboxylate group of Glu354 and Glu333 (right).

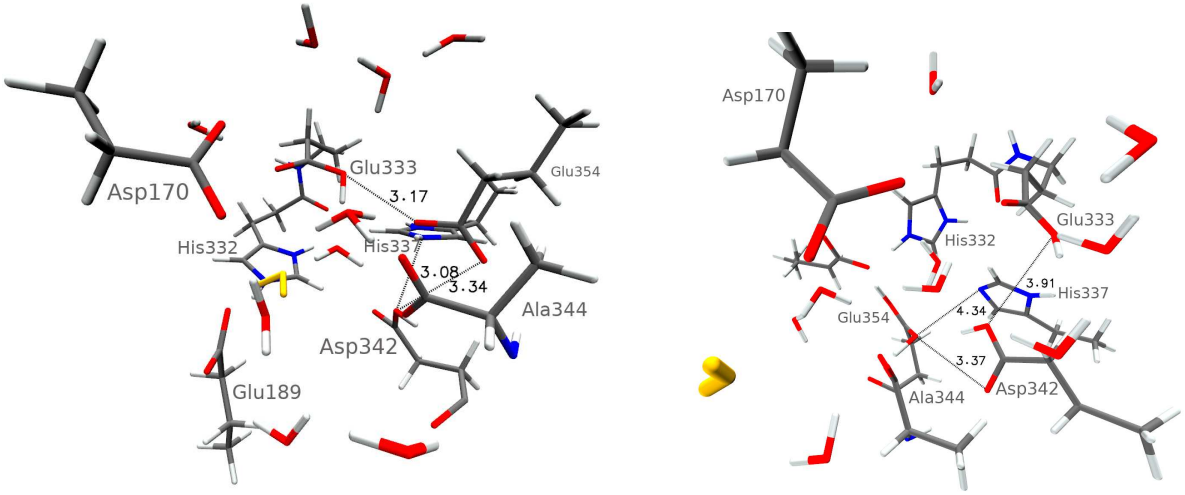

Figure 8: Structure of the cavity with an additional third water molecule inside the cavity after optimization with DFT of system 6 (left) and a snapshot of an *ab-initio* MD run of system 0 (right). The additional water molecule is shown in yellow. Selected amino acid distances are indicated with dotted lines.

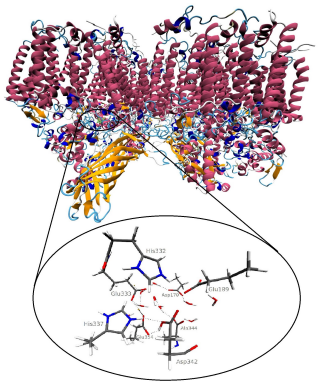

Figure 9: Table of Contents: Different protonation patters of the photosystem II without the water-oxidizing complex (apo-PSII) have been investigated computationally. Static and dynamic density functional theory simulations show which proton distributions lead to agreement with experimental X-ray data, thus paving the way for further investigations of the photoassembly process of photosystem II.